Fibers and Polymers 2022, Vol.23, No.1, 1-9
DOI 10.1007/s12221-021-3276-8

ISSN 1229-9197 (print version)
ISSN 1875-0052 (electronic version)

Biocompatible Gradient Chitosan Fibers with Controllable Swelling and Antibacterial Properties

Shangpeng Liu[1,2,3†], Yi Yu[1†], Shasha Jiang[5†], Jiwei Li[1,2,3*], Shuang Wang[4], Shaojuan Chen[1], and Jianwei Ma[1*]

[1]*Industrial Research Institute of Nonwovens and Technical Textiles, College of Textiles and Clothing, Qingdao University, Qingdao 266071, China*
[2]*Shandong Center for Engineered Nonwovens, Qingdao 266071, China*
[3]*National Manufacturing Innovation Center of Advanced Dyeing and Finishing Technology, Taian 271000, China*
[4]*Department of Biochemistry and Microbiology, Qingdao University Medical College, Qingdao 266071, China*
[5]*Department of Pathogenic Biology, Qingdao University Medical College, Qingdao 266071, China*
(Received March 24, 2021; Revised May 7, 2021; Accepted May 11, 2021)

Abstract: This study developed a partially water-soluble carboxymethyl chitosan (PWCS) fibers by ethanol-water exhaustion method. Sodium carboxylate was successfully introduced into chitosan fibers, as evidenced by FTIR, which enhanced natural chitosan water solubility. SEM-EDS revealed that the sodium carboxylate groups presented in a gradient distribution from the exterior to the interior of the PWCS fibers, which leads to a controllable swelling performance. Moreover, the PWCS fibers had excellent antibacterial ability against *S. aureus* and *E. coli* bacteria comparing with origin CS fibers. The cytotoxicity assay (CCK-8) and fluorescence staining confirmed that all developed samples showed non-toxicity towards MRC-5 and exhibited a surprising promoting effect on cell proliferation, corroborating their biocompatibility. Besides, due to its excellent controllable water selling ability and protonated amine groups, the PWCS fibers possessed an efficient hemostatic performance. In conclusion, PWCS fibers could become a promising material in hemostatic and wound healing applications.

Keywords: Chitosan fibers, Controllable swelling, Antibacterial, Hemostatic, Biocompatible

Introduction

At present, there is increasing attraction in the uncontrolled bleeding problem because hemorrhage is a major cause of high mortality on the battlefields, traffic accidents and operations, and so on [1-3]. Thus, many researchers are devoted to developing the proper hemostatic materials to control the bleeding. Currently, there are many available hemostatic materials, such as oxidized cellulose, zeolite powders and medical gelatin sponges [4-6]. However, these materials also have some disadvantages. For example, zeolite powder lacks biocompatibility and can influence blood capillaries, which leads to thrombosis [7-9]. Moreover, gelatin sponges easily results in the second damages and inflammation due to adhesion of the wound [10].

Chitosan is the deacylated form of chitin extracted from crustacean shells, which has good biodegradability, biocompatibility, antibacterial, hemostatic activity, and low toxicity, having numerous applications in the medical field [11,12]. Currently, chitosan-based hemostats have emerged to be one of the most promising bleeding controlling materials [13,14]. However, pure chitosan fibers have poor solubility in aqueous solvents, which causes the limitation of further applications in the biomedical field, especially in hemostatic materials. For this, many improvements include the variations in the physical form, the manipulation of micro/nano-structures, the incorporation of biological or artificial agents, and the synthesis of new chitosan derivatives that have been made in the use of chitosan as hemostatic material [15].

Previous studies have proved that the water absorption ability can enable hemostats to absorb water from the blood, thus rapidly concentrating on platelets, erythrocytes, and clotting factors [16,17]. For example, water soluble chitosan has been coated on to oxidized cellulose, and its performance as a hemostat agent has been studied and improved performance in terms of degradation rate and hemostasis. Hemamalini *et al*. [18] reported that the red blood cells and platelet deposition were higher in soluble acid chitosan than water-soluble chitosan, which is beneficial for hemorrhage application. Nonetheless, the chitosan materials with water soluble possess a small water contact angle, and after they absorb biofluids until saturation, excessive biofluids are controlled on the surface of the wound. Unabsorbed biofluids would build a moist environment, and cause microbial invasion and bacterial colonization. Furthermore, overhydrate dressing would lead to tissue damage with adhesion of wound [19,20].

In this study, chitosan fibers were modified by the ethanol-water exhaustion method to obtain partially water-soluble carboxymethylated chitosan fibers for hemostatic materials.

*Corresponding author: Jiweili@qdu.edu.cn
*Corresponding author: 915286867@qq.com
†These authors contribute equally to this work.

Scanning electron microscopy (SEM)-Energy dispersive spectrometer (EDS) was performed to confirm carboxymethylated chitosan fiber's gradient structure. The physical properties, biocompatibility, antibacterial property, and hemostatic performance were tested to evaluate chitosan fiber's application potential in hemostatic materials.

Experimental

Materials

Chitosan fibers were gifted from Qingdao Jifa Group Co., Ltd., China. Sodium chloroacetate ($ClCH_2COONa$, AR, 98 %, MW=116.48) and ethanol were purchased from shanghai Aladdin biochemical technology Co., Ltd., China. Sodium hydroxide (NaOH, AR) was purchased from Shanghai Wokai Biotechnology Co., Ltd., China. The CCK-8 assay kit was purchased from GlpBio (USA). The *Staphylococcus aureus* (CMCC26003) and *Escherichia coli* (ATCC25922) were purchased from Shanghai Luwei Technology Co., Ltd., China. The primary human embryonic lung fibroblasts (MRC-5) were purchased from the Department of Key Laboratory of Molecular Virology of Shandong Province. Deionized water was obtained from the experiment.

Preparation of Carboxymethyl Chitosan

Carboxymethyl chitosan fibers were synthesized according to the previously reported [21]. Firstly, 20 g NaOH powder was added to 200 m*l* ethanol solution of 65 % and stirred until the powder was dissolved thoroughly. Next, chitosan fibers (20 g) were added to the prepared solution. Finally, the $ClCH_2COONa$ was mixed at different weight ratios (weight ($ClCH_2COONa$): weight (NaOH)) of 1:1, 4:3, 2:1 and 4:1, respectively (the corresponding samples were labeled as CS-1, CS-2, CS-3, CS-4). The reaction was kept at a thermostat water bath under a temperature of 60 °C for 10 min. After the reaction, the processed fibers were washed twice times with 75 % (v/v) aqueous ethanol solution and dehydrated with 95 % (v/v) ethanol aqueous solution. The final samples were dried at 20 °C.

Material Characterizations

The morphological characterization was observed by a scanning electron microscopy (SEM) (TESCAN VEGA3, China). The chemical structure was determined using a Fourier transform infrared (FTIR, NICOLET iS0, USA) spectroscopy in the room temperature transmission mode. Thermal stability was characterized using thermal gravimetric analysis (TGA). The test was conducted on a TG209F3 instrument at a heating rate of 10 °C/min from 25 °C to 800 °C in the nitrogen flow.

The X-ray diffraction analysis (XRD, Rigaku SmartLab, Japan) was conducted to characterize these samples' crystal structure. The range of 2θ was performed from 5 ° to 80 ° with steps of 3 °.

The swelling property of CS and PWCS was evaluated in deionized water at room temperature. Briefly, the dried weight of samples was measured as W_0 (about 0.1 g) and immersed in deionized water for 24 h. Then, the swollen samples were taken out from deionized water, and the extra water was removed using filter paper (GE Biotechnology (Hangzhou) Co., Ltd.) before weighed (W_t). Each sample was repeated three times. The swelling degree was calculated from the following formula:

$$\text{Swelling degree (\%)} = (W_t - W_0)/W_0 \times 100\ \%$$

The Vitro Biocompatibility Characterization

0.1 g samples were irradiated by Ultraviolet (UV) for 30 min and immersed in Dulbecco's modified Eagles medium (DMEM) to prepare the extract of different concentrations (25 %, 50 %, and 100 %). In vitro cytotoxicity of CS, CS-1, CS-2, CS-3, and CS-4 was evaluated using a cell counting kit-8 (CCK-8). In brief, the 100 μ*l* of MRC-5 at the density of 2×10^6/m*l* was seeded into 96-well culture plates and incubated in a culture medium with 5 % humidified carbon dioxide (CO_2) at 37 °C for 24 h. Then, the culture mediums were removed. And the prepared extract of different concentrations was added to each well and cultured for 24 h, 48 h, respectively. After co-cultivation, 10 μ*l* of CCK-8 assay was added into each well and incubated for another 2 h at 37 °C. A group without extract is named as the blank. The absorbance at 450 nm was measured using a microplate reader and calculated according to the following equation:

$$\text{Cell viability} = (OD_{sample} - OD)/(OD_{blank} - OD) \times 100\ \%$$

(OD represents the absorbance of cell culture fluid). Each sample was repeated three times.

Further, the cell morphology was observed to evaluate the cell viability by fluorescence staining [22]. Specifically, after the all samples (CS, CS-1, CS-2, CS-3 and CS-4), PBS solution (the control group) and cell (MRC-5) were co-cultured for 48h, the mixture was washed three times with PBS and cells were fixed for 10 min with 4 % formaldehyde at room temperature, followed by rinsing with PBS. Next, they were stained with FTIC for 1 h under the dark condition and washed with PBS three times. Then they were stained with DAPI for 15 min and washed with PBS three times to remove residual DAPI and photographed using a confocal laser scanning microscope.

Antibacterial Activity Assessment

The antibacterial activity of carboxymethyl chitosan was assessed with *Staphylococcus aureus* (*S. aureus,* Gram-positive) and *Escherichia coli* (*E. coli*, Gram-negative) according to the disc diffusion method [30]. Briefly, the 200 μ*l* of bacterial suspensions (the final concentration of 1×10^6 CFU/m*l*) was added to the solid agar medium and

spread over using a glass spreading rod. Next, 0.1 g of samples were placed on agar plates' surface and kept close contact with agar. To be measured accurately, all samples were pressed into a disc (7 mm of diameter) using the Tablet press (1.75 tones with load), and then the same procedure was performed. After incubation for 24 h at 37 °C, the inhibition zone area was measured by ImageJ 1.46r. Each experiment was performed three times.

In vitro Blood Cells Adhesion Test

SEM observed the blood cells and platelet adhesion with fresh blood with anticoagulant citrate sodium (9:1). Different fibers were immersed in whole anticoagulant blood and incubated for 1 h at room temperature. Then all samples were washed three times, with 0.9 wt% NaCl solution to remove the non-adhered blood cells. The fibers' surface cells were immobilized with 2.5 % (w/v) glutaraldehyde for 30 min. The samples were washed three times with saline solution and deionized water, respectively, to remove residual NaCl. Finally, the samples were dried at a freezer dryer overnight, and the SEM images were obtained after gold spraying.

Hemostatic Testing

The whole blood clotting experiment was carried out according to previous literature [20]. Briefly, the weighted samples (0.2 g, CS-2 and CS-3) were placed into a centrifuge tube, and the 1 m*l* of fresh blood from eight-week-old KM mice was added to the test tube. $CaCl_2$ (30 μ*l*, 0.25 mol/*l*) was added, and then clotting time was measured. The untreated CS was used as a control group. Each sample was repeated three times.

Results and Discussion

Chemical and Graded Structure Characterization

Figure 1a showed the FTIR spectra of CS and PWCS. The infrared spectra of CS displayed characteristic peaks at 3440 cm^{-1} (superposition of -OH and $-NH_2$ stretching), 2879 cm^{-1} (C-H absorption peak), 1155 cm^{-1} (-OH absorption peak on the C6 position of chitosan), and 1598 cm^{-1} and 1654 cm^{-1} (corresponding to the $-NH_2$ bending absorption). The -OH absorption peak at 1155 cm^{-1} and $-NH_2$ bending absorption peak at 1654 cm^{-1} became weak, indicating the reaction took place on the -OH group of C6 and $-NH_2$ group of C2 for CS (Figure 1b). Furthermore, Compared with CS, two new absorption peaks appeared at 1411 cm^{-1} and 865 cm^{-1} on the different carboxymethyl chitosan, which was attributed to C=O's stretching vibration in COOH groups. The result confirmed that the carboxymethyl group was successfully introduced onto chitosan.

We investigated the surface morphology of the original CS and modified CS with SEM. Figure 2a revealed that the original CS's surface was smooth and regular, and the modified CS showed a rough surface with many fragments due to the different levels of carboxymethylation. Compared with CS-1, CS-2, and CS-3, the fragment on the CS-4 fibers' surface was more and denser. Furthermore, the EDS analysis was employed to confirm the distribution of -COONa group on the fibers. Figure 2b showed that the Na element's content first reduced and then increased along the red line on the cross-section of CS-1, CS-2, CS-3, and CS-4. In other words, the density of -COONa group gradually decreased from surface to core along the radial direction. The results indicated that the reaction occurred on the surface and then gradually into the core of fibers after the treatment of $ClCH_2COONa$ with different concentration, which led to higher -COONa group content on the surface than that inside of the fiber.

Physical Characterization

The XRD patterns of CS, CS-1, CS-2, CS-3 and CS-4 were displayed in Figure 5a. The pure chitosan showed the two broad peaks at 10.09 ° and 20.22 °, corresponding to (020) and (110) planes, respectively. Under carboxymethylation, the major peak intensity at 20.22 ° not only decreased, but the peak at 10.09 ° almost disappeared [23,24]. The results indicated that the crystal structure of chitosan was damaged

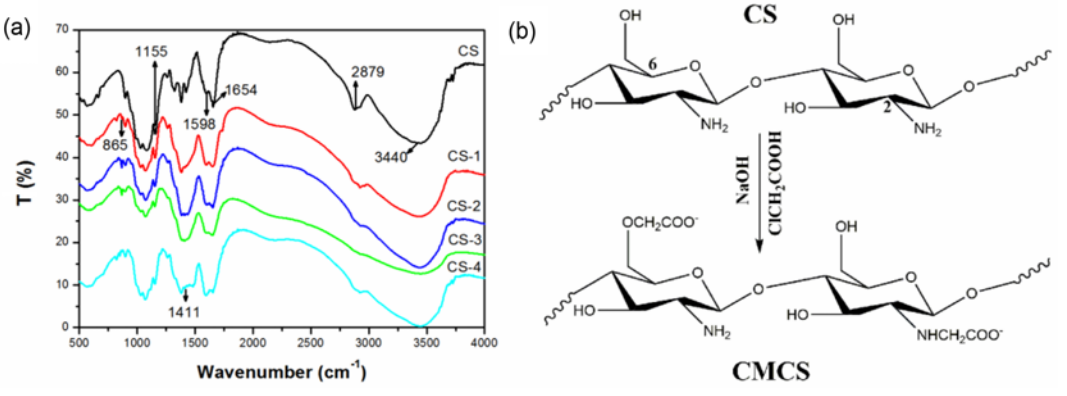

Figure 1. (a) FTIR spectra of CS, CS-1, CS-2, CS-3 and CS-4 and (b) schematic representation of carboxymethylation reaction.

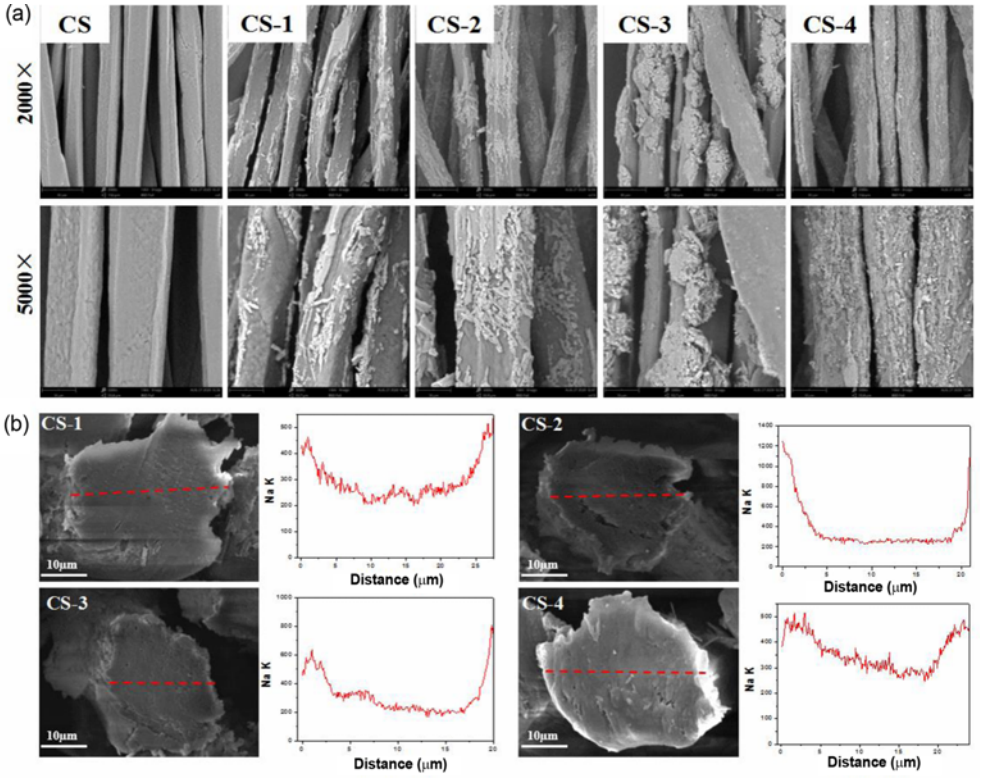

Figure 2. (a) The surface SEM images of original CS and PWCS and (b) SEM of cross-section and corresponding distribution of Na element along the radial direction.

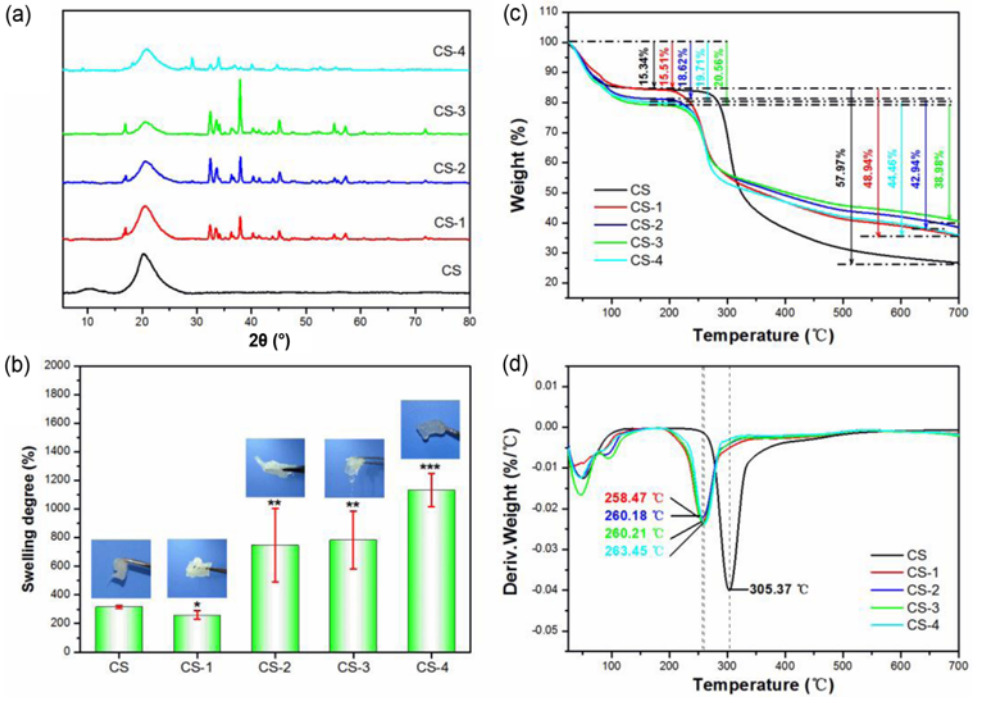

Figure 3. (a) XRD curves of CS and CS-1, CS-2, CS-3 and CS-4, (b) swelling degree of CS, CS-1, CS-2, CS-3 and CS-4 and the illustrations are the corresponding digital photographs after immersion (*, **, *** indicates $P>0.05$, $P<0.05$ and $P<0.01$ compared with CS respectively). (c) TGA curves of CS (black) and CS-1 (red), CS-2 (blue), CS-3 (green) and CS-4 (cyan) and (d) corresponding DTG curves. (For interpretation of the references to colour in this figure legend, the reader is referred to the web version of this article.)

seriously. The introduction of -COONa groups weakened the hydrogen-bond interaction between the hydroxy on the C2 and C3 position and C6 position of chitosan. Therefore, CS-1, CS-2, CS-3, and CS-4 presented perfect solubility comparing with CS.

The benign swelling ability is important for hemostatic materials, which is beneficial to absorb the exudates from the wound site and the aggregation of blood cells on the surface of swollen materials accelerates the blood coagulation [25-28]. Figure 3b showed that with increasing chloroacetate concentration, the swelling degree of different carboxymethyl productions increased gradually. CS-1 had no statistical difference with CS after absorbing water and appeared slight gel on the surface of CS and CS-1. The swelling degree of CS-2 and CS-3 was found to be 747.32 % and 783.8 %, respectively. Moreover, part of the surface materials formed a gel, and fibrous structure cores were still observed. CS-4 lost its original fibrous structure and totally formed a gel, and its swelling degree was 1133.3 %. The above results proved that the controllable introduction of sodium carboxylate (-COONa) groups derived the carboxymethyl materials water-soluble partially.

TGA and DTG analyzed thermal stability and degradation of CS, CS-1, CS-2, CS-3, and CS-4. Figure 3c showed that the thermal degradation of CS and different carboxymethyl productions mainly occurred in two stages. The first stage's weight loss was due to the evaporation of adsorbed water in the range of 25-150 °C. Figure 1a illustrated that the mass loss of pure CS (15.34 %) was less than different productions after carboxymethylation (15.51 %, 18.62 %, 19.71 %, and

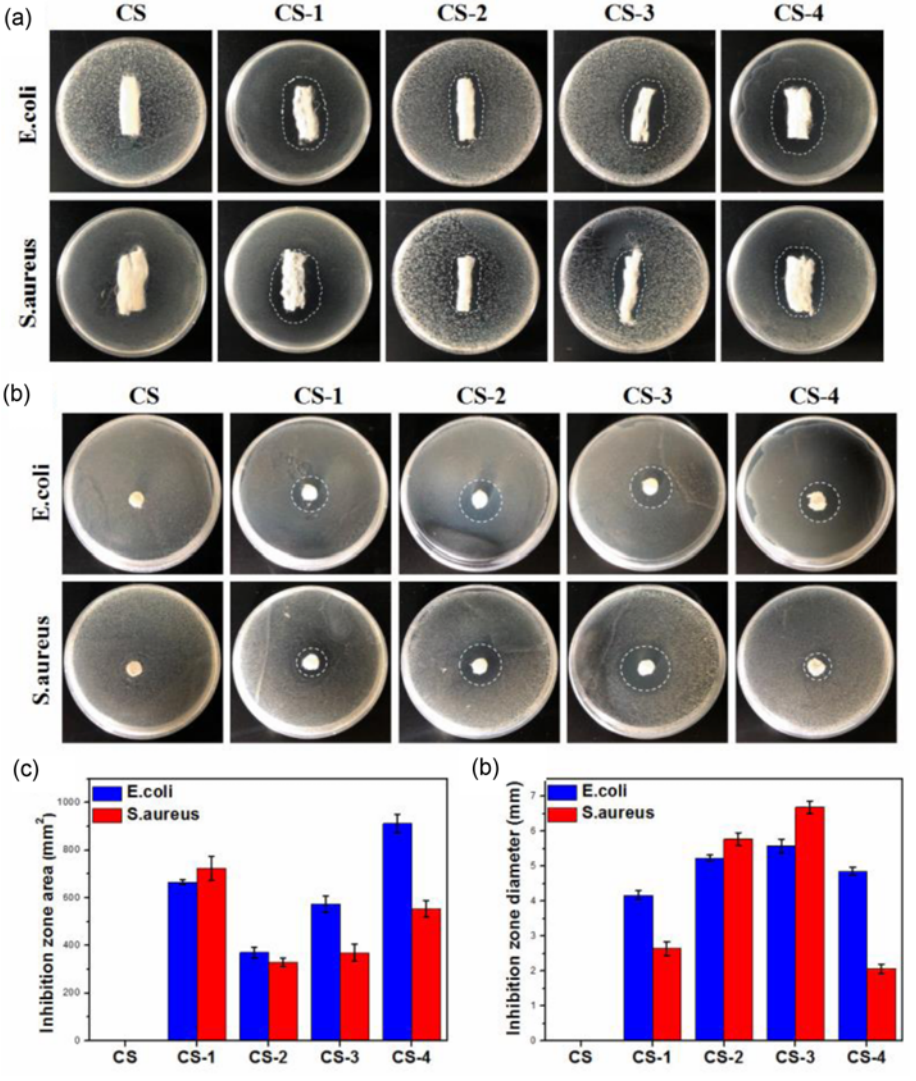

Figure 4. Antibacterial activity of CS, CS-1, CS-2, CS-3 and CS-4. (a) and (b) typical photographs of the inhibition zone with 0.1 g sample and disc, respectively. (c) The zone area of inhibition with 0.1 g sample. (d) The zone diameter of inhibition with disc sample. (For interpretation of the references to colour in this figure legend, the reader is referred to the web version of this article.)

20.56 %, respectively), which was in agreement with the results of swelling degree. The second stage of weight loss was related to the change of chemical structure when the first step included the sugar ring dehydration and degradation and scission of ether linkages in the range of 250-400 °C, and the next step was attributed to the breakage of glucosamine in the range of 400-700 °C [29]. Furthermore, as DTG showed, the maximum weight loss point for CS was 305.37 °C, and the weight loss was 57.97 % at the second stage (Figure 3d). Compared with CS, the maximum weight loss point for CS-1, CS-2, CS-3, and CS-4 reduced about 45 °C, and the thermal stability of carboxymethyl chitosan decreased, which resulted from the presence of new substituents in the chitosan derivatives. However, the weight loss of chitosan derivatives (48.94 %, 42.94 %, 38.98 %, and 44.46 %, respectively) was less than the 57.97 % of CS in the second stage, which was due to the substituents attached to the amine group in the chitosan derivatives. The results indicated that carboxymethylation reaction occurred on -NH_2 group of C2 for CS.

Antibacterial Capacity Evaluation

Bacterial infection mainly causes wound infection [30-34]. Thus, we assessed the prepared samples' antibacterial activity against *S. aureus* and *E. coli*. Figure 4a and b showed the inhibition zone of all samples in contact with *S. aureus* and *E. coli*. It's worth noting that other prepared samples exhibited a good antibacterial property except CS fibers, which is due to that the antibacterial effect of natural chitosan will be presented by protonating the amino group under acidic conditions [35-37]. Therefore, the carboxymethylation reaction did not only promote the solubility but accelerated the release of the amino group, which can damage the negatively charged components like proteins, phospholipids and kill bacteria.

Besides, There was little persuasive for the fluffy fibrous sample to determine the antibacterial effect due to the contact area's difference with bacteria. We further measured the inhibition zone diameter with the disc by tablet press. Figure 4d showed that the inhibition zone values of prepared samples against *E. coli* were respectively 4.2, 5.2, 5.6, and 4.9 mm for CS-1, CS-2, CS-3, and CS-4, and 2.6, 5.8, 6.7 and 2.1 mm of corresponding values against *S.aureus*. These prepared samples presented a perfect antibacterial property comparing with natural chitosan. In brief, the carboxymethylation reaction gives PWCS excellent antibacterial

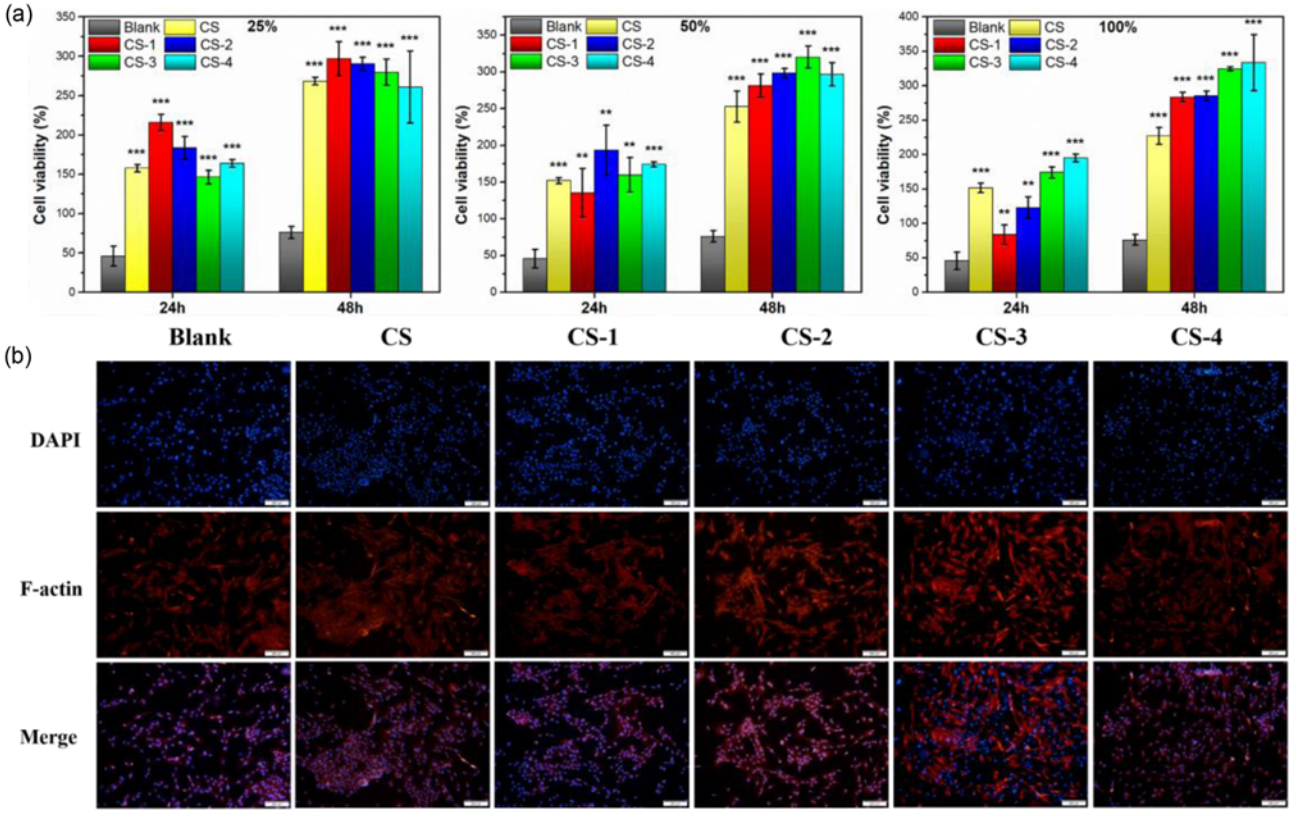

Figure 5. (a) Cytotoxicity on MRC-5 cells after co-culturing for 48 h with the different concentrations of extracts of materials (**, *** indicates P<0.05 and P<0.01 compared with blank group respectively) and (b) fluorescence staining of cells at 48 h of culture with the different materials. (For interpretation of the references to colour in this figure legend, the reader is referred to the web version of this article.)

properties to be suitable for hemostatic material.

Cytotoxicity and Morphology Analyses

The cytocompatibility of CS and PWCS was assessed by fluorescence staining and CCK-8 assays. As shown in Figure 5a, compared to the untreated cells (blank group), the viability of MRC-5 cells cultured with the concentration of all samples extract, increasing from 25 % to 100 %, was higher, and the corresponding viability values were all above approximately 200 % after 48 h incubation. These surprising results suggested that the CS and prepared CS extract had non-toxicity and were beneficial to cell growth and proliferation. Therefore, we supposed that all materials possessed the promoting effect on the proliferation of MRC-5 cells. Figure 5b showed that the cell morphologies treated with materials extract of 100 % for 48 h, and these cells grew well and exhibited a polygonal shape with filopodia and lamellipodia [38]. In a word, the above results revealed that PWCS fibers are suitable to use as hemostatic materials due to its excellent compatibility.

Hemostatic Performance

SEM observed the cell's adhesion and morphology of hemocytes and platelets on the fibers. The SEM images showed that none of the red blood cells were found on the pure CS fibers, and only a few red blood cells were absorbed on the CS-1. The results indicated that CS and CS-1 had no evident effect on the blood cells' physiological action when they contacted the fibers. Compared with the two formers, the surface of CS-2, CS-3, and CS-4 after carboxymethylation aggregated and adhered to many blood cells, and blood cells were agglutinated and highly deformed [39-41]. The

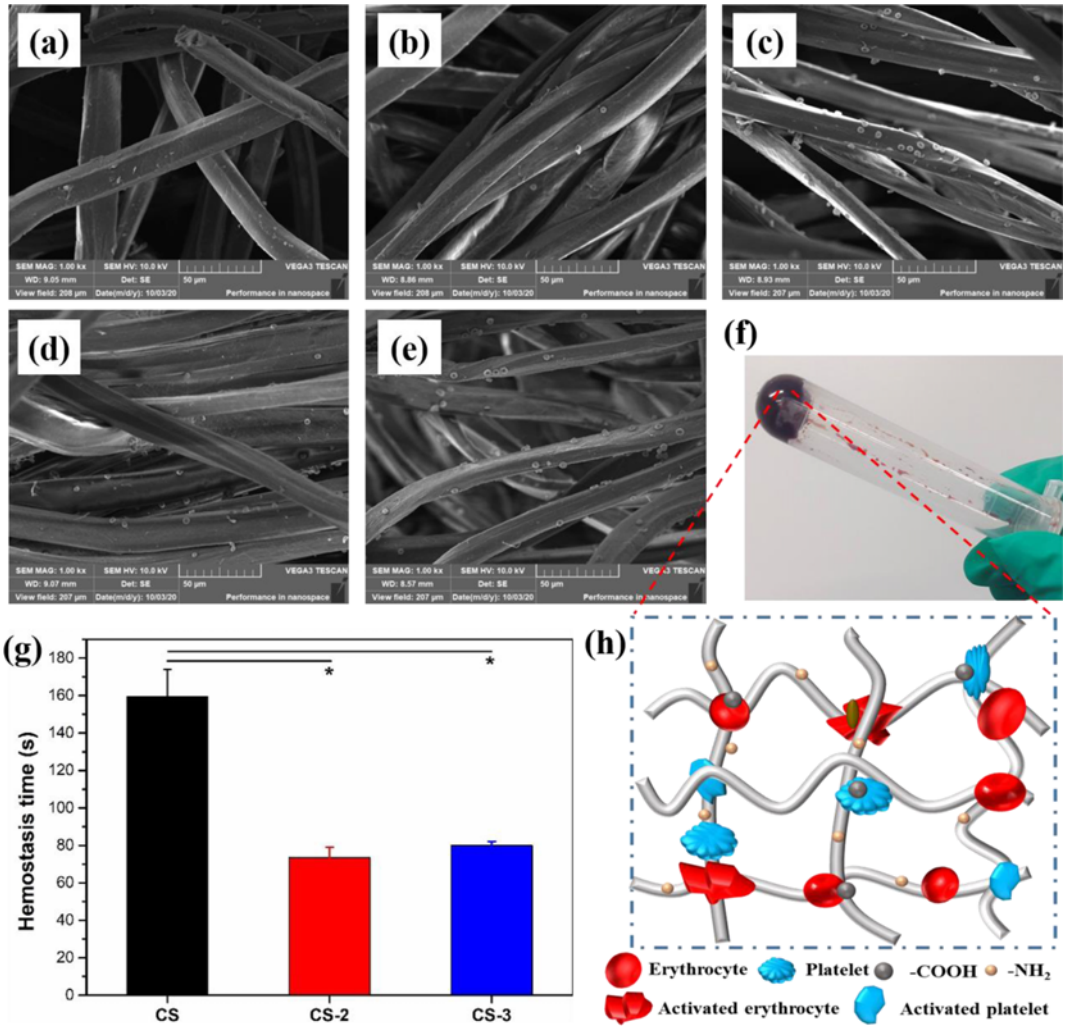

Figure 6. (a) SEM images of blood cell and platelet adhesion on the surface of CS (a), CS-1 (b), CS-2 (c), CS-3 (d) and CS-4 (e). (f) Images of CS-2/whole blood mixture after coagulation. (g) The hemostatic time of CS, CS-2 and CS-3. (h) Schematic illustration of hemostasis process. *$p<0.05$ compared to control. (For interpretation of the references to colour in this figure legend, the reader is referred to the web version of this article.)

phenomena attributed to the introduced carboxyl groups, protonated amine groups, and the release of quaternary ammonium groups of CS-2, CS-3 and CS-4 surface could attract and activate the platelets [42-45]. The above results demonstrated that CS-2, CS-3, and CS-4 could promote platelets' adsorption and activation capabilities and achieve blood coagulation. Further, considering the swelling ability results, CS-2, and CS-3 promoted blood clotting and prevented adherence with wound due to over absorbent samples.

Above the results, CS-2 and CS-3 can be used as hemostatic materials because of its gradient structure. Therefore, CS-2 and CS-3 were chosen for the vitro hemostatic assay. Compared with CS samples, CS-2 and CS-3 samples' hemostasis time showed a significant difference ($P<0.05$) and could reduce the hemostatic time due to the fast adsorption and platelets' activation (Figure 6g). In particular, CS-2 and CS-3 accelerated the hemostatic time to (73.5±5.5 s) and (80±2 s) in comparison with CS (159.5±14.5 s). The results demonstrated that CS-2 and CS-3 samples had promising hemostatic properties.

Conclusion

We have developed partially water-soluble carboxymethylated chitosan fibers (PWCS) with excellent biocompatibility and antibacterial property. SEM-EDS analysis proved the gradient structure of PWCS. Moreover, the CS-2, CS-3, and CS-4 fibers exhibited greater water-soluble performance than CS fibers. Furthermore, CS-2 and CS-3 showed controlled swelling property, which prevents overhydrate and bacterial colonization. And overhydrate dressing would lead to tissue damage with adhesion of wound. In the antibacterial efficacy assessment, two operations revealed that the developed samples displayed satisfactory antibacterial ability against *E. coli* and *S. aureus* for preventing wound infection. Furthermore, in vitro blood cells adhesion test, the surface of CS-2, CS-3, and CS-4 fibers absorbed many blood cells with deformation, which accelerated blood coagulation. Blood clotting in vitro indicated that CS-2 and CS-3 fibers performed better than original CS fibers. The cytotoxicity evaluation (CCK-8) confirmed the non-toxicity for MRC-5. With all these performances, the gradient structure can provide a potential strategy for chitosan fibers as hemostatic materials in the future.

Acknowledgment

This work was partially supported by the China Postdoctoral Fund (NO. 2018M632618), National Key Research and Development Program of China (NO. 2017YFB0309805-02), National Natural Science Foundation of China (NO. 82001754) and National Key R&D Program of China (NO. 2018YFA0900802).

References

1. Y. L. Wang, Y. N. Zhou, X. Y. Li, J. Huang, F. Wahid, C. Zhong, and L. Q. Chu, *Int. J. Biol. Macromol.*, **156**, 252 (2020).
2. K. M. Rao, M. Suneetha, G. T. Park, A. G. Babu, and S. S. Han, *Int. J. Biol. Macromol*., **155**, 71 (2020).
3. Z. A. Raza, U. Bilal, U. Noreen, S. A. Munim, S. Riaz, M. U. Abdullah, and S. Abid, *Fiber. Polym.*, **20**, 1360 (2019).
4. L. Qu, X. Guo, M. Tian, and A. Lu, *Fiber. Polym.*, **15**, 1357 (2014).
5. K. Y. Lu, Y. C. Lin, H. T. Lu, Y. C. Ho, S. C. Weng, M. L. Tsai, and F. L. Mi, *Carbohydr. Polym.*, **206**, 664 (2019).
6. M. Lei, W. Huang, J. Sun, Z. Shao, W. Duan, T. Wu, and Y. Wang, *J. Mol. Liq.*, doi: 10.1016/j.molliq.2020.113135 (2020).
7. Z. Wu, W. Zhou, W. Deng, C. Xu, Y. Cai, and X. Wang, *ACS Appl. Mater. Interfaces*, **12**, 20307 (2020).
8. S. Liu, Z. Zheng, S. Wang, S. Chen, J. Ma, G. Liu, B. Wang, and J. Li, *Carbohydr. Polym*., **224**, 115175 (2019).
9. Y. Ge, J. Tang, H. Fu, Y. Fu, and Y. Wu, *Fiber. Polym.*, **20**, 698 (2019).
10. K. Ravishankar, K. M. Shelly, R. P. Desingh, R. Subramaniyam, A. Narayanan, and R. Dhamodharan, *ACS Sustainable Chem. Eng.*, **6**, 15191 (2018).
11. M. A. Asghar, R. I. Yousuf, M. H. Shoaib, and M. A. Asghar, *Int. J. Biol. Macromol.*, **160**, 934 (2020).
12. M. Alavi and A. Nokhodchi, *Carbohydr. Polym.*, **227**, 115349 (2020).
13. D. Wang, N. Zhang, G. Meng, J. He, and F. Wu, *Colloids Surf B Biointerfaces*, **194**, 111191 (2020).
14. J. M. Souza, M. Henriques, P. Teixeira, M. M. Fernandes, R. Fangueiro, and A. Zille, *Fiber. Polym.*, **20**, 922 (2019).
15. F. Cheng, Y. Wu, H. Li, T. Yan, X. Wei, G. Wu, J. He, and Y. Huang, *Carbohydr. Polym.*, **207**, 180 (2019).
16. L. Wang, Z. Luo, J. Yan, Z. Ban, M. Yang, M. Qi, Y. Xu, F. Wang, and L. Li, *Ultrason Sonochem*., doi: 10.1016/j.ultsonch.2020.105184 (2020).
17. F. Tang, F. Gao, W. Xie, S. Li, B. Zheng, M. Ke, and J. Huang, *Carbohydr. Polym.*, **235**, 115949 (2020).
18. T. Hemamalini, N. Vikash, P. Brindha, M. Abinaya, and V. R. G. Dev, *Int. J. Biol. Macromol.*, **147**, 493 (2020).
19. J. M. He, Y. D. Wu, F. W. Wang, W. L. Cheng, Y. D. Huang, and B. Fu, *Fiber. Polym.*, **15**, 504 (2014).
20. E. Fakhri, H. Eslami, P. Maroufi, F. Pakdel, S. Taghizadeh, K. Ganbarov, M. Yousefi, A. Tanomand, B. Yousefi, S. Mahmoudi, and H. S. Kafil, *Int. J. Biol. Macromol.*, **162**, 956 (2020).
21. X. Chen and H. Park, *Carbohydr. Polym*., **53**, 355 (2003).
22. A. Plaza, B. Merino, N. Del Olmo, and M. Ruiz-Gayo, *Br. J. Pharmacol.*, **176**, 2678 (2019).
23. H. E. Salama and M. S. Abdel Aziz, *Int. J. Biol. Macromol.*, **163**, 649 (2020).
24. E. S. Hosseini, L. Manjakkal, D. Shakthivel, and R. Dahiya, *ACS Appl. Mater. Interfaces*, **12**, 9008 (2020).

25. X. Yao, G. Zhu, P. Zhu, J. Ma, W. Chen, Z. Liu, and T. Kong, *Adv. Funct. Mater*., doi: 10.1002/adfm.201909389 (2020).
26. M. Lei, W. Huang, J. Sun, Z. Shao, T. Wu, J. Liu, and Y. Fan, *Appl. Clay Sci*., doi: 10.1016/j.clay.2020.105637 (2020).
27. Z. Kharat, M. Sadri, and M. Kabiri, *Fiber. Polym.*, doi: 10.1007/s12221-021-0490-3 (2021).
28. T. Hussain, R. Masood, M. Umar, T. Areeb, and A. Ullah, *Fiber. Polym*., **17**, 1749 (2016).
29. T. Hemamalini, N. Vikash, P. Brindha, M. Abinaya, and V. R. Giri Dev, *J. Bioact. Compat. Polym.*, **35**, 92 (2020).
30. S. Liu, J. Li, S. Zhang, X. Zhang, J. Ma, N. Wang, S. Wang, B. Wang, and S. Chen, *ACS Appl. Bio Mater.*, **3**, 848 (2019).
31. S. Liu, J. Ma, S. Wang, S. Chen, B. Wang, and J. Li, *Mater. Lett.*, doi: 10.1016/j.matlet.2019.126570 (2019).
32. M. Yin, Y. Wang, Y. Zhang, X. Ren, Y. Qiu, and T. Huang, *Carbohydr. Polym*., doi: 10.1016/j.carbpol.2019.115823 (2019).
33. M. Niu, X. Liu, J. Dai, H. Jia, L. Wei, and B. Xu, *Fiber. Polym.*, **11**, 1201 (2010).
34. Y. Ge and M. Ge, *Fiber. Polym.*, **16**, 308 (2015).
35. A. Ullah, S. Ullah, T. Areeb, M. Umar, P. D. Nam, R. Masood, S. Park, and I. S. Kim, *Fiber. Polym.*, **21**, 2494 (2020).
36. M. Lu, S. Yu, Z. Wang, Q. Xin, T. Sun, X. Chen, Z. Liu, X. Chen, J. Weng, and J. Li, *Eur. Polym. J*., doi: 10.1016/j.eurpolymj.2020.109821 (2020).
37. H. Ma, Y. Zhao, Z. Lu, R. Xing, X. Yao, Z. Jin, Y. Wang, and F. Yu, *Int. J. Biol. Macromol.*, **164**, 986 (2020).
38. Y. Li, X. Liu, L. Tan, Z. Cui, X. Yang, Y. Zheng, K. W. K. Yeung, P. K. Chu, and S. Wu, *Adv. Funct. Mater*., doi: 10.1002/adfm.201800299 (2018).
39. Y. Huang, X. Zhao, Z. Zhang, Y. Liang, Z. Yin, B. Chen, L. Bai, Y. Han, and B. Guo, *Chem. Mater*., **32**, 6595 (2020).
40. M. Li, Z. Zhang, Y. Liang, J. He, and B. Guo, *ACS Appl. Mater. Interfaces*, **12**, 35856 (2020).
41. E. P. Oliveira, T. S. O. Souza, D. Y. Okada, L. H. S. Damasceno, and R. B. Moura, *Chem. Eng. J*., doi: 10.1016/j.cej.2020.124988 (2020).
42. M. Shin, J. H. Ryu, K. Kim, M. J. Kim, S. Jo, M. S. Lee, D. Y. Lee, and H. Lee, *ACS Biomater Sci. Eng.*, **4**, 2314 (2018).
43. Y. Wang, D. Xiao, Y. Zhong, Y. Liu, L. Zhang, Z. Chen, X. Sui, B. Wang, X. Feng, H. Xu, and Z. Mao, *Int. J. Biol. Macromol.*, **160**, 18 (2020).
44. D. Yan, S. Hu, Z. Zhou, S. Zeenat, F. Cheng, Y. Li, C. Feng, X. Cheng, and X. Chen, *Int. J. Biol. Macromol*., **107**, 463 (2017).
45. J. Qu, X. Zhao, Y. Liang, T. Zhang, P. X. Ma, and B. Guo, *Biomaterials*, **183**, 185 (2018).